Regular Article

PHYSICAL CHEMISTRY RESEARCH
Published by the
Iranian Chemical Society
www.physchemres.org
info@physchemres.org

Phys. Chem. Res., Vol. 6, No. 2, 399-414, June 2018
DOI: 10.22036/pcr.2018.105287.1432

KCl Promoted Cobalt-iron Nanocatalysts Supported on Silica: Catalytic Performance and Characterization in Fischer-Tropsch Synthesis

M. Feyzi[a,b,*], M. Joshaghani[a] and S. Nadri[a]

[a]*Faculty of Chemistry, Razi University, P. O. Box: 6714967346, Kermanshah, Iran*

[b]*Nanoscience & Nanotechnology Research Center (NNRC), Razi University, P. O. Box: 6714967346, Kermanshah, Iran*

(Received 9 December 2017, Accepted 5 April 2018)

The SiO_2 supported cobalt-iron nano catalysts were prepared by the sol-gel method. This research investigated the effects of (Co/Fe) wt%, different Co/Fe ratios at different temperatures and loading of KCl wt% for Fisher-Tropsch synthesis (FTS). The results showed that the catalyst containing 50 wt% (Co/Fe)/SiO_2 (Co/Fe ratio is 70/30) promoted with 0.6 wt% KCl is an optimal nano catalyst for conversion CO + H_2 to a range of hydrocarbons especially light olefins. The results also indicated that optimal operating conditions for optimal nano catalyst are 250 °C, and H_2/CO molar ratio 2/1 under 1 bar of pressure. Characterization of catalyst precursors and calcined catalysts were performed by different methods such as: powder X-ray diffraction (XRD), transmission electron microscopy (TEM), N_2 physisorption and thermal analysis methods such as thermal gravimetric analysis (TGA) and differential scanning calorimetry (DSC).

Keywords: Fischer-Tropsch synthesis, Syngas, Co/Fe nano catalyst, Sol-gel method

INTRODUCTION

Undoubtedly, the main goal of the Fischer-Tropsch process is not only introduction of cheap, efficient and selective catalysts for production of fuels and heavier hydrocarbons from lighter hydrocarbons, but also is to produce the products with high quality. The Fischer-Tropsch synthesis (FTS) [1-3] can be carried out either in high (> 350 °C, HTFT) or in low (< 250 °C, LTFT) temperatures [4,5]. The HTFT process is carried out at slurry reactor, and produces light olefins, while the LTFT process could be carried out at both slurry and fixed-bed reactors and produce mainly paraffinic heavy hydrocarbons. Due to the thermodynamic and kinetic limitations of the reaction, few catalysts are able to amplify the heavier fraction of hydrocarbons. Among them, Ru-based catalysts show higher activity, however, they are very expensive [6-9]. Nickel-based catalysts could be employed but their efficiencies in hydrogenation process which compete with FTS, and produce CH_4 as an undesirable byproduct [10,11]. Both Fe- and Co-based catalysts individually have advantages and disadvantages [12-19]. Therefore, effort to couple them in the hope to bring forth a more efficient catalyst having parents' advantages is of great importance. These bimetal catalysts should be inserted into a highly porous support to increase the surface area and mechanical stability of the catalysts and prohibition of the catalyst sintering. In addition to porosity, shape and size of the pores are critical secondary factors. The best supports are those that are simply manipulated to produce optimum texture properties. Silica [20,21] and γ-alumina [22,23] are good in this regard particularly in the Sol-Gel preparation method [24]. The purpose of this paper is to investigate the influence of catalyst composition and operational conditions on the FTS performance and product selectivity. Characterization of all catalysts were carried out by powder X-ray diffraction (XRD), transmission electron microcopy (TEM), N_2 physisorption and thermal analysis methods such

*Corresponding author. E-mail: Dalahoo2011@yahoo.com

as thermal gravimetric analysis (TGA) and differential scanning calorimetry (DSC).

EXPERIMENT

Typical Procedure for Preparation of Catalysts

A series of Co-Fe/SiO_2 catalysts with different loadings of Fe and Co was prepared. An appropriate amount of starting materials including cobalt nitrate [$Co(NO_3)_2.6H_2O$] and iron nitrate [$Fe(NO_3)_3.9H_2O$] were dissolved in ethanol at 60 °C, separately and mixed well with each other. The required amounts of TEOS [$Si(C_2H_5O)_4$] as silica source were dissolved in ethanol at 60 °C and then gradually added to the cobalt-iron containing solution to produce 30, 40, 50, 60, 70 and 80 wt% of Co/Fe = 1/1 (based on SiO_2 wt%) mixture solutions, respectively. An ethanol solution of oxalic acid ($C_2H_2O_4.2H_2O$, appropriate amount for TEOS hydrolysis) was added to a mixed solution under constant stirring to obtain a gel form. The gel was dried in an oven (120 ºC, 12 h) to give a material denoted as the catalyst precursor. The promoted catalysts were then prepared by the incipient wetness impregnation method by adding different loadings (0.2-1.2 wt%) of KCl to cobalt– iron precursor. The obtained precursors was then dried at 110 °C for 12 h and calcined at 400 °C for 6 h.

Characterization of Catalysts

The XRD patterns were obtained using a Bruker axs D8 Advance diffractometer. Scans were taken with a 2θ step size of 0.02 from 4 to 70^o and a counting time of 1.0 s using Cu K_α radiation source generated at 40 kV and 30 mA. N_2 physisorption was performed using a NOVA 2000 BET instrument. Prior to the measurements, all catalyst samples were slowly degassed at 150 °C for 4 h under inert N_2 atmosphere. Then, the samples were transferred to the adsorption unit to determine the textural properties. The TGA and DSC were carried out using simultaneous thermal analyzer STA 1500+ under a flow of dry air. The temperature was gradually raised from 25 °C to 650 °C using a linear programmer at a heating rate of 5 °C min^{-1}. TEM image was carried out using a Hitachi H-7500 (120 kV). The sample for TEM image was prepared by ultrasonic radiation of the catalyst in ethanol solvent. The obtained suspension was dropped on to a carbon-coated copper grid.

Fischer-Tropsch Reaction

Catalytic performance test was carried out in a fixed bed stainless steel reactor at different operation conditions (Fig. 1). All catalysts were activated (reduced) for 16 h period on line in pure hydrogen (1 bar) at a temperature of 400 ºC at flow rate of 30 ml min^{-1}. Meshed catalyst (1.0 g) was loaded in the reactor (30 cm length and internal diameter is 7 mm). Feed and products were analyzed on-line using a Varian gas chromatograph (Star 3600CX) whose detector for gas analysis is thermal conductivity detector (TCD) and a chromosorb column. The liquid hydrocarbon products were analyzed using a Varian CP 3800 with a Petrocol Tm DH100 fused silica capillary column and a flame ionization detector (FID). The conversion percentage of CO is calculated based on the CO fraction forming carbon-containing products, according to Eq. (1)

:

$$\text{CO conversion } (\%) = \frac{C_{CO_{in}} - C_{CO_{out}}}{C_{CO_{in}}} \times 100 \quad (1)$$

where, n_i is the number of carbon atoms in product i, M_i is the percentage of product i, and M_{CO} is the CO % in the syngas feed. The selectivity (S) of product i, is based on the total number of carbon atoms in the product and therefore is defined as:

$$S_i\ (\%) = \frac{n_i M_i}{\sum n_i M_i} \times 100 \quad (2)$$

RESULTS AND DISCUSSION

Effect of Cobalt-iron Weight Percentage

As a starting point of our investigation, the effect of different wt% of cobalt/iron (based on the SiO_2 weight) under the same reaction conditions (H_2/CO = 2/1, GHSV = 1200 h^{-1}, P = 1 bar and T = 220 °C) was investigated. As Table 1 shows, the catalyst activity based on CO conversion increases linearly with decreasing wt% of (Co/Fe) while the selectivity toward undesirable methane and CO_2 decreases till 50 wt% of Co/Fe and then increases markedly. According to the obtained results, the catalyst containing 50

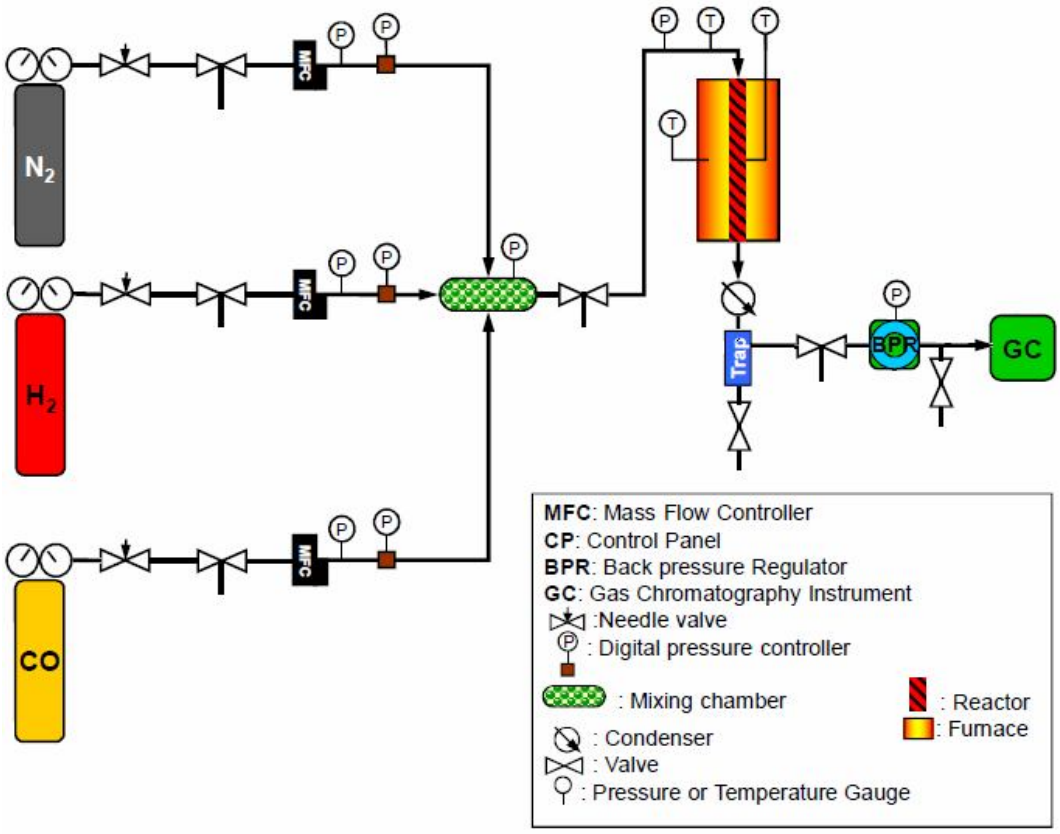

Fig. 1. Schematic representation of the testing system for the catalyst and used reactor.

Table 1. Effect of Different wt% of (Co/Fe) on FTS Performance and Product Selectivity

	wt%(Co/Fe)					
	30	40	50	60	70	80
CO conversion (%)	41.5	40.9	40.0	37.0	36.4	34.5
CH_4	28.8	27.1	25.6	27.6	28.1	29.7
C_2-C_3 paraffin	13.3	14.0	15.1	14.3	14.1	13.7
C_2-C_3 olefin	17.8	18.1	19.6	17.8	17.4	15.4
C_4-C_5 paraffin	9.2	9.1	9.5	9.1	8.5	8.5
C_4-C_5 olefin	10.5	10.7	12.0	9.3	8.6	8.3
C_6+	12.0	13.3	12.9	13.7	14.0	14.0
CO_2	8.4	7.7	5.3	8.2	9.3	10.4

Reaction conditions: H_2/CO = 2/1, GHSV = 1200 h^{-1}, P = 1 bar and 220 °C.

Table 2. Textural Properties of the Cobalt/Iron Precursors

wt% (Co/Fe)	Specific surface area ($m^2 g^{-1}$)			Pore diameter (Å)		Pore volume ($cm^3 g^{-1}$)	
	BET	BJH	DH	BJH	DH	BJH	DH
30	139.3	141.6	137.5	16.8	16.3	0.27	0.29
40	136.9	139.1	136.9	17.2	17.5	0.32	0.30
50	134.7	132.6	134.1	18.3	18.6	0.38	0.36
60	123.2	126.1	124.8	16.8	17.0	0.31	0.34
70	108.5	106.4	104.7	13.6	13.9	0.26	0.24
80	103.4	105.7	105.3	12.7	13.1	0.23	0.25

Table 3. Textural Properties of the Cobalt/Iron Catalysts

wt% (Co/Fe)	Specific surface area ($m^2 g^{-1}$)			Pore diameter (Å)		Pore volume ($cm^3 g^{-1}$)	
	BET	BJH	DH	BJH	DH	BJH	DH
30	156.8	155.3	151.5	17.4	16.8	0.60	0.56
40	149.3	153.4	154.1	15.9	18.3	0.64	0.63
50	147.8	150.1	148.3	16.6	17.4	0.64	0.68
60	138.2	139.6	137.7	12.2	13.1	0.56	0.59
70	132.6	130.4	131.3	11.3	10.7	0.47	0.45
80	124.7	126.2	125.9	10.4	11.7	0.41	0.46

Table 4. Textural Properties of the Cobalt/Iron Catalysts after the Test

wt% (Co/Fe)	Specific surface area ($m^2 g^{-1}$)			Pore diameter (Å)		Pore volume ($cm^3 g^{-1}$)	
	BET	BJH	DH	BJH	DH	BJH	DH
30	139.7	137.1	142.3	14.8	14.1	0.48	0.51
40	138.1	141.5	139.4	13.7	14.8	0.41	0.45
50	144.5	145.9	143.1	14.3	16.0	0.58	0.61
60	129.4	127.3	128.6	10.6	11.4	0.44	0.40
70	119.5	120.7	117.6	9.5	8.9	0.39	0.36
80	111.7	110.8	112.2	8.2	8.5	0.32	0.34

wt% of (Co/Fe) presents the best catalytic performance compared to the other tested catalysts at the mentioned operational conditions. This catalyst showed the highest selectivity towards olefinic products (C_2-C_5) and the low selectivity towards methane and CO_2. Thus, this catalyst was selected as the optimal catalyst. The specific surface area (BET, DH and BJH methods), pore volume and pore diameter of the precursors and calcined catalysts (before and after reaction) are given in Tables 2, 3 and 4, respectively. A relatively high surface area of the precursor is mainly due to solvent evaporation which makes a porous surface of high surface area. The surface area of the calcined catalysts is higher than the corresponding precursors which is mainly due to gas evolution from the solid during of calcination process. It can be seen that the increase of (Co/Fe) wt% results in a linear decrease in the catalyst surface area which is in comformity with catalyst activity based on CO conversion. On the other hand, the pore volume increases with increasing the cobalt/iron ratio to reach a maximum at 50 wt% of (Co/Fe), and then decreases with further increasing of cobalt/iron ratio which is in agreement with selectivity trend. The calcined catalysts were examined with powder X-ray diffraction to investigate the effect of loadings of cobalt/iron on the phase structure. Typical XRD patterns for the precursors and calcined forms of the catalysts are shown in Figs. 2 and 3, respectively. The precursors prepared from different cobalt-iron ratios were largely found to be amorphous and silicate phases (Fig. 2). These amorphous phases make the other phases such as iron hydroxi phases undetectable. In addition, the calcined catalysts contain the oxide phases of Co_3O_4 (cubic), Fe_2O_3 (cubic, tetragonal), $CoFe_2O_4$ (cubic), Co_2SiO_4 (orthorhombic), and Fe_2SiO_4 (cubic), however, the relative diffracted intensities, especially for main phases, were different and noticeale (Fig. 3).

Taking into account that the optimum catalyst was the 50 wt% of (Co/Fe)/SiO_2 catalyst, in order to identify the changes happened to this catalyst during the reactions, and also for detection of the phases formed, this catalyst after the test was characterized by XRD (Fig. 4). The phase of catalyst after the test (T = 220 °C) was found to be metallic iron in the form of cubic structure, and Fe_3O_4 (cubic), Fe_2SiO_4 (cubic), Co_3C (orthorhombic), Fe_3C (orthorombic), CoO (cubic) phases. As shown, the tested catalyst has oxidic and iron carbide phases, both of which have been generally accepted to be the most likely active phase for FTS performance [25-29]. One of the affecting parameters on catalytic performance was catalyst particle size. This parameter could be calculated by Scherer-equation [30,31]. Table 5 summarizes the results obtained from XRD. It was found that the crystallite size of catalysts were decreased with increasing of SiO_2 (decreasing wt% Co/Fe) content which clearly confirm the dispersion effect of SiO_2 that is support of catalyst. From the results presented in Table 5, it is clear that the catalyst particle size was in nano dimension. It was found that cobalt particle size had a strong impact on cobalt catalyst selectivity; the olefin selectivity decrease with increasing the particle size of catalyst [32-35]. Our resultsare in agreement with these reports and lower olefins selectivity were obtained for higher cobalt loading contain higher particle size.

The optimal catalyst containing 50 wt% of (Co/Fe)/SiO_2 was characterized with TEM (Fig. 5). As clearly seen in this figure, the size of particles is 35-50 nm, that is in agreement with what was obtained fromthe Scherrer equation. The precursor was subjected to thermal gravimetric analysis and differential scanning calorimetery. As shown in Fig. 6, the TGA/DSC curves of 50 wt% (Co/Fe)/SiO_2 catalyst precursor exhibit a three-step weight loss. The first step at the temperature below 150 °C was attributed to the evaporation of residual moistures of the support and loss of physisorbed waters. The second step at the temperature, between 150 and 280 °C, was the decomposition of oxalate phases and removal of hydrate and bound waters. The third weight loss occurs above 280 °C corresponds to the full decomposition of all oxalate phases and the formation of stable cobalt and iron oxides.

Effect of Cobalt/iron Weight Ratio

The influence of the cobalt/iron weight ratio at various reaction temperatures on the catalytic performance of cobalt/iron nano catalyst containing 50 wt% (Co/Fe)/SiO_2 under atmospheric pressure, H_2/CO = 2/1 and GHSV = 1200 h^{-1} were studied (Tables 6-10). The results showed that variation of cobalt/iron ratio (90/10-20/80) at different temperatures (220-260 °C) resulted in different products selectivity. However, for the catalyst containing 50 wt% (Co/Fe)/SiO_2 with cobalt/iron = 70/30 at T = 250 °C, the

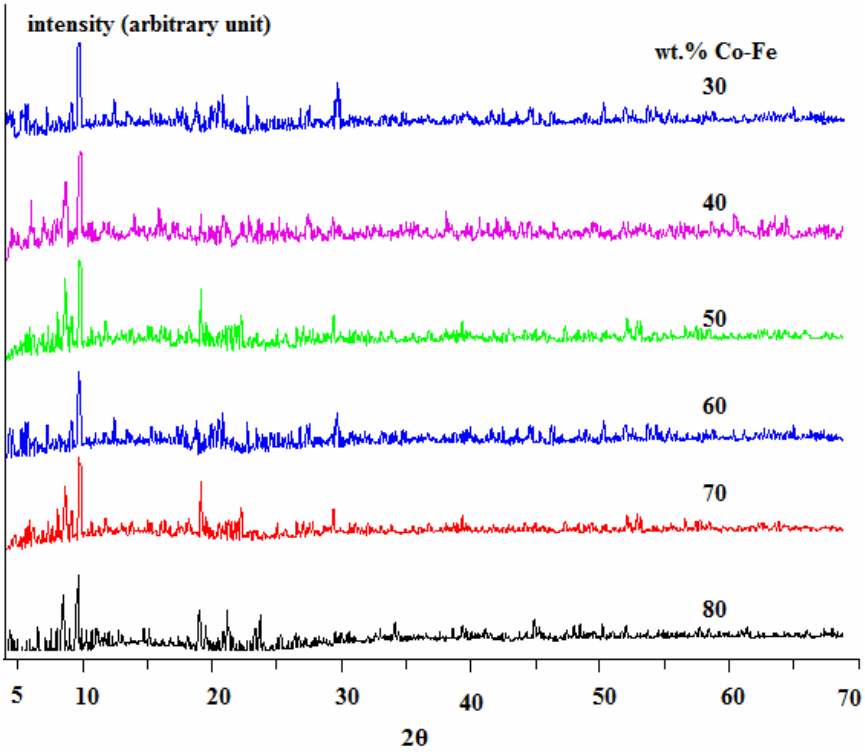

Fig. 2. XRD patterns of catalyst precursors with different wt% of (Co/Fe).

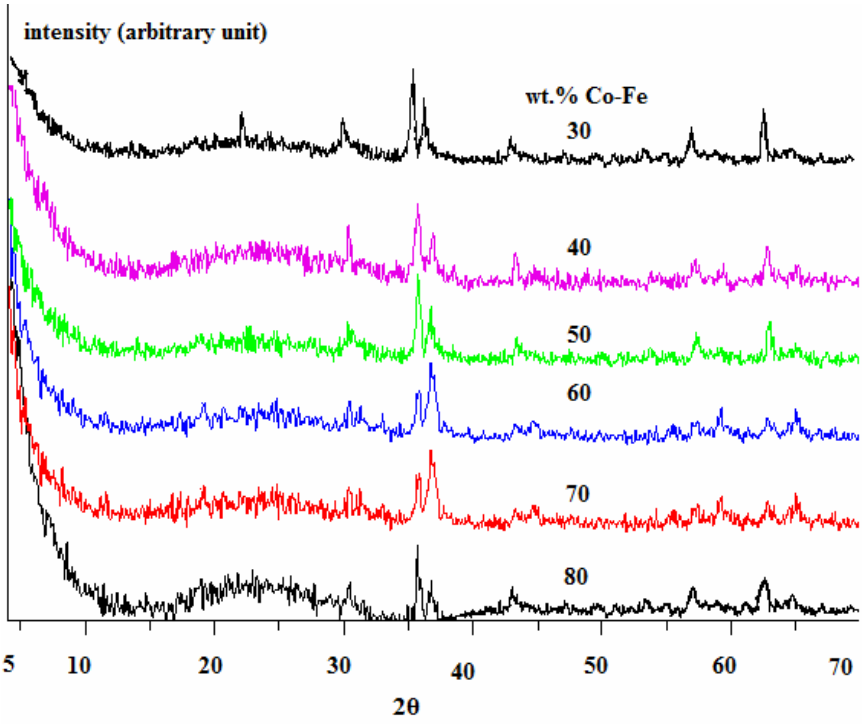

Fig. 3. XRD patterns of catalysts with different wt% of (Co/Fe).

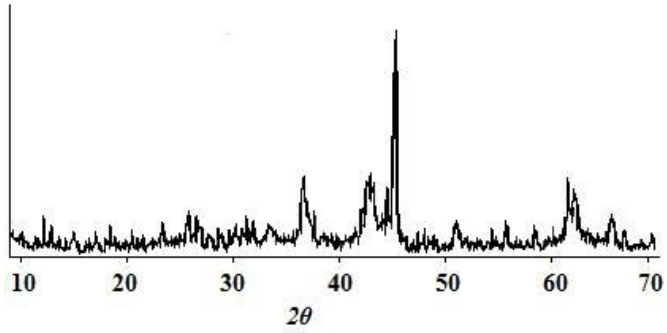

Fig. 4. XRD pattern of catalyst with 50 wt% (Co/Fe)/SiO_2 after the test.

Table 5. Average Size of the Particles of Studied Catalysts

wt% (Co/Fe)	2θ	Size (nm)
30	37	36
40	37	38
50	37	40
60	37	44
70	37	51
80	37	54

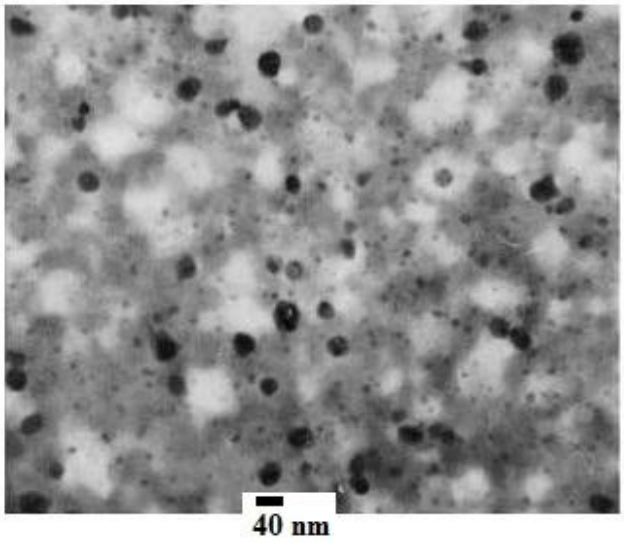

Fig. 5. TEM image of calcined catalyst containing 50 wt% (Co/Fe)/SiO_2.

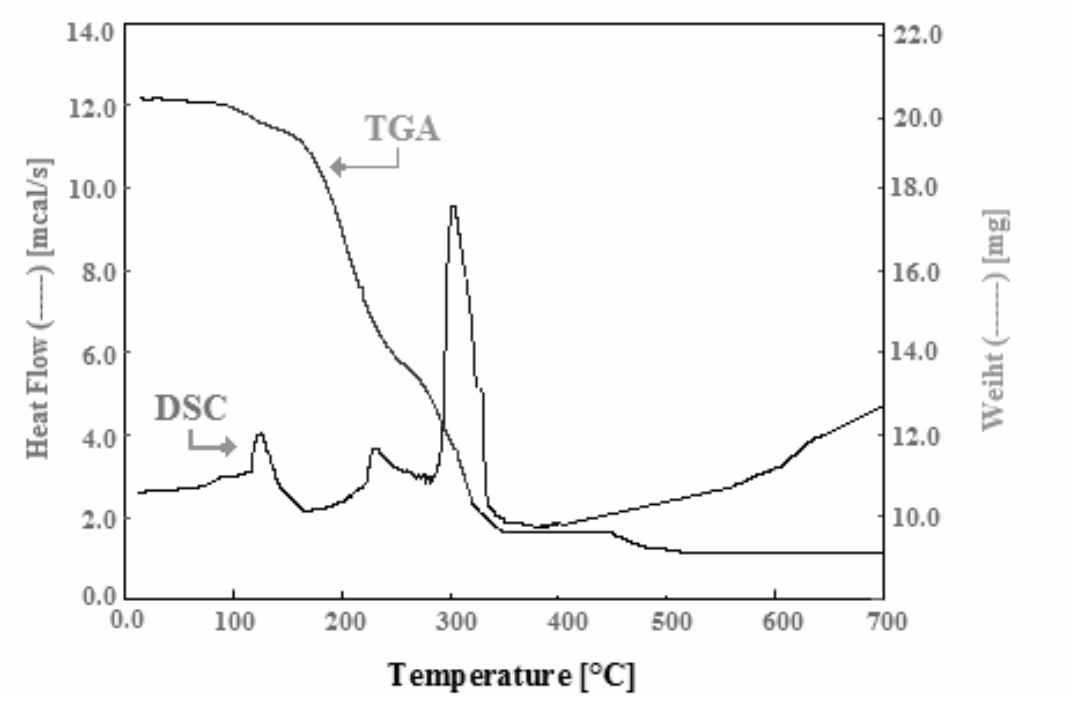

Fig. 6. TGA/DSC curves for the 50 wt% (Co/Fe)/SiO_2 catalyst precursor.

Table 6. Effect of Different Co/Fe Ratios on the Catalytic Performance at 220 °C

	Co/Fe Ratio (%)							
	90/10	80/20	70/30	60/40	50/50	40/60	30/70	20/80
CO conversion (%)	35.7	37.2	38.0	39.2	40.0	41.3	42.0	43.3
CH_4	25.1	24.3	23.0	26.0	25.6	25.3	26.5	27.4
C_2-C_3 paraffin	14.9	15.5	15.5	12.8	15.1	15.1	13.9	13.6
C_2-C_3 olefin	17.0	19.4	20.9	21.0	19.6	17.3	20.5	19.7
C_4-C_5 paraffin	10.0	9.2	9.0	8.1	9.5	11.0	10.4	9.2
C_4-C_5 olefin	10.4	10.6	12.0	12.4	12.0	10.8	9.0	9.5
C_6+	17.1	15.7	14.9	15.0	12.9	14.8	13.8	14.3
CO_2	5.5	5.3	4.7	4.7	5.3	5.7	5.9	6.3

Reaction conditions: $H_2/CO = 2/1$, GHSV = 1200 h^{-1} and P = 1 bar.

Table 7. Effect of Different Co/Fe Ratios on the Catalytic Performance at 230 °C

	Co/Fe Ratio (%)							
	90/10	80/20	70/30	60/40	50/50	40/60	30/70	20/80
CO conversion (%)	37	38.9	41.9	42.2	43.2	43.6	45.7	46.8
CH_4	22.4	21.6	19.4	22.5	23.7	25.2	26.1	26.4
C_2-C_3 paraffin	15	15.5	16.1	13.3	14.1	14.3	14.6	13.4
C_2-C_3 olefin	17.5	18.9	21.2	22.2	20.6	20.5	20.4	21.5
C_4-C_5 paraffin	10.6	10.1	9.8	8.8	9.6	9.3	8.7	9.4
C_4-C_5 olefin	11.5	11.8	12.4	13.1	12.8	11.7	10.3	9.6
C_6+	17.8	17.1	16.8	15.6	14.3	14.8	14.2	13.7
CO_2	5.2	5	4.3	4.5	4.9	5.5	5.7	6

Reaction conditions: $H_2/CO = 2/1$, GHSV = 1200 h^{-1} and P = 1 bar.

Table 8. Effect of Different Co/Fe Ratios on the Catalytic Performance at 240 °C

	Co/Fe Ratio (%)							
	90/10	80/20	70/30	60/40	50/50	40/60	30/70	20/80
CO conversion (%)	45.5	48.6	55	55.5	53.7	56.4	57	58.1
CH_4	28.2	26.8	21.1	25.1	26.3	26.9	28.5	29.0
C_2-C_3 paraffin	18.4	17.9	18.3	18.2	16.9	16.2	17.0	18.3
C_2-C_3 olefin	16.2	19.3	21.5	19.1	19.0	18.2	16.3	17.4
C_4-C_5 paraffin	8.5	7.9	9.8	9.3	9.1	8.2	9.2	7.2
C_4-C_5 olefin	9.3	9.9	10.2	8.4	8.1	7.1	6.9	7.9
C_6+	11.9	11.1	14.0	13.9	14.1	15.6	13.5	10.9
CO_2	7.5	7.1	5.1	6.0	6.5	7.8	8.7	9.3

Reaction conditions: $H_2/CO = 2/1$, GHSV = 1200 h^{-1} and P = 1 bar.

Table 9. Effect of Different Co/Fe Ratios on the Catalytic Performance at 250 °C

	Co/Fe Ratio (%)							
	90/10	80/20	70/30	60/40	50/50	40/60	30/70	20/80
CO conversion (%)	45.5	48.6	55	55.5	53.7	56.4	57	58.1
CH_4	28.2	26.8	21.1	25.1	26.3	26.9	28.5	29.0
C_2-C_3 paraffin	18.4	17.9	18.3	18.2	16.9	16.2	17.0	18.3
C_2-C_3 olefin	16.2	19.3	21.5	19.1	19.0	18.2	16.3	17.4
C_4-C_5 paraffin	8.5	7.9	9.8	9.3	9.1	8.2	9.2	7.2
C_4-C_5 olefin	9.3	9.9	10.2	8.4	8.1	7.1	6.9	7.9
C_6+	11.9	11.1	14.0	13.9	14.1	15.6	13.5	10.9
CO_2	7.5	7.1	5.1	6.0	6.5	7.8	8.7	9.3

Reaction conditions: $H_2/CO = 2/1$, GHSV = 1200 h^{-1} and P = 1 bar.

Table 10. Effect of Different Co/Fe Ratios on the Catalytic Performance at 260 °C

	Co/Fe Ratio (%)							
	90/10	80/20	70/30	60/40	50/50	40/60	30/70	20/80
CO conversion (%)	43.5	47.4	50.1	51.8	51.5	50	49.2	50.5
CH_4	30.7	30.1	29.6	33.4	34.5	35.4	35.7	37.5
C_2-C_3 paraffin	15.7	14.8	14.1	13.8	14.5	13.8	12.9	12.4
C_2-C_3 olefin	17.3	18.7	20.1	17.3	15.7	15.8	16.0	14.2
C_4-C_5 paraffin	12.0	13	10.9	10.6	10.1	9.8	9.2	6.9
C_4-C_5 olefin	7.9	7.1	6.8	7.2	7.9	6.9	6.8	7.3
C_6+	8.5	8.0	9.9	8.8	8.0	9.0	9.1	10.5
CO_2	8.0	8.3	8.6	8.8	9.3	9.3	10.3	11.2

Reaction conditions: $H_2/CO = 2/1$, GHSV = 1200 h^{-1} and P = 1 bar.

catalyst activity (based on CO conversion to products) was higher than other tested catalyst at different temperatures, and also the selectivities toward undesired products of methane and CO_2 were lower. Therefore, cobalt/iron = 70/30 ratio at 250 °C was chosen as the optimum catalyst. This result is in agreement with previous reports that the reaction temperature should not be too low or high [36]. At low reaction temperatures, the conversion of CO is low and so it causes a low catalytic performance. On the other hand, increasing the reaction temperature leads to the formation of amounts of coke. The CO conversion increased linearly with increasing temperature, similar results were also obtained by Schulz and Claeys [37,38]. Both the CO conversion and CO_2 formation followed the same trends as the FTS reaction, and almost presented a linear correlation with increasing reaction temperature. Bukur *et al*. [39] investigated a precipitated iron catalyst in a fixed bed reactor under a variety of process conditions, and also observed that selectivity of light olefins was high at the reaction temperature of around 300 ºC during FTS. The XRD technique was carried out to identify the changes in phases of catalyst which may occures during the reaction. The optimum catalyst after the test was characterized by XRD and its phases were found to be Fe_3O_4 (cubic), FeC_2 (orthorhombic), CoO (cubic), Fe_2SiO_4 (cubic), $CoFe_2O_4$ (cubic), and Co_2SiO_4 (orthorhombic). As shown, the tested catalyst has oxidic and iron carbide phases. In course the reaction, metallic iron phases converted to iron carbide, and then, the iron carbide may be oxidized to iron oxide. It is well known that the iron carbide phases are active for FTS, and oxidic species are responsible for production of olefins [40,41]. The selectivity toward CO_2 increases with increasing the loading of iron which is in agreement with literature about the efficacy of iron catalysts toward water-gas shift [42-44].

Effect of Percentage of KCl

To study the effect of KCl impregnation on the catalytic performance, different KCl wt%, from 0.2-1.2 wt%, were considered and all tested under atmospheric pressure, H_2/CO = 2/1, T = 250 °C and GHSV = 1200 h^{-1}. Both potassium and chlorine were reported to have positive [45,46], negative [47,48], or no effect on the catalyst performance, depending on a number of different factors such as the support material, loading amount of K and Cl, and reaction conditions. As shown in Table 11, the activity of catalyst containing 50 wt% (Co/Fe)/SiO_2 (Co/Fe ratio is 70/30) increases with increasing wt% of KCl and achieve a maximum activity of 70.9% for 0.6 wt% KCl, and then decreases with further increasing of KCl wt%. At these conditions, methan and CO_2 production decreases till 0.6 wt% KCl then increases markedly. In overall, impregnation with 0.6 wt% KCl was selected as optimal. The effect of chlorine on the Fischer-Tropsch synthesis over iron and cobalt catalysts was investigated by Barrault [49] who reported a significant increase in the selectivity to light olefins, a marked drop in methane production, and increase in activity of catalysyt. They found that a weak poisoning of iron catalysts by halogen ions suppresses secondary hydrogenation of olefins, resulting in an increased olefin selectivity, in agreement with what has been obtained in this study. The BET surface areas, pore volumes and average pore diameters of the incorporated catalyst with KCl are listed in Table 12. The decreased pore volume and BET specific surface area are observed when the catalyst is loaded with different wt% of KCl, possibly due to pore filling and/ or pore blocking of mesopores during the impregnation step.

Effects of Total Pressure

The effect of total pressure was considered for 50 wt% (Co/Fe)/SiO_2 (Co/Fe ratio is 70/30) promoted with 0.6 wt.% KCl nano catalyst. The catalyst performance shows two opposite trend with respect to pressure (Table 13). With increasing the pressure, the CO conversion decreases slowly while selectivity toward heavy hydrocarbons increases (at same operational conditions of H_2/CO = 2/1, GHSV = 1200 h^{-1} and 250 ºC). This behavior indicates that many parameters including economical considerations should be involved in the pressure optimization. High total selectivity toward heavy hydrocarbons (C_6+, C_4-C_5 olefin and C_4-C_5 paraffin) at higher pressures may be due to more condensation of hydrocarbons, which are normally in the gaseous state at atmospheric pressure [50]. However, lower CO conversions are probably due to increasing the importance of diffusion step and/or changes in the morphology of the catalyst. Therefore, in this study, p = 1 bar was considered to be the optimum total pressure because

Table 11. Effect of Different Contents of KCl on the Catalytic Performance

	wt% KCl						
	0.0	0.2	0.4	0.6	0.8	1.0	1.2
CO conversion (%)	55	57.1	60.6	70.9	64.2	52.3	45.5
CH_4	21.1	20.6	19.4	13.3	18.1	18	19.5
C_2-C_3 paraffin	18.3	20	20.8	21.8	21	20.7	22
C_2-C_3 olefin	21.5	23.5	26.6	28.3	23.2	20	18.2
C_4-C_5 paraffin	9.8	9.3	8.8	10.8	10.3	10.8	8.6
C_4-C_5 olefin	10.2	9.9	10.1	11.2	9.3	9	8.3
C_6+	14	11.8	10.1	11.7	12.3	14.2	14.2
CO_2	5.1	4.9	4.2	2.9	5.8	7.3	9.2

Reaction conditions: $H_2/CO = 2/1$, GHSV = 1200 h^{-1}, P = 1 bar and 250 °C.

Table 12. The BET Surface Areas, Pore Volumes and Average Pore Diameters of the Catalysts Promoted with KCl

	Specific surface area (m^2g^{-1})			Pore diameter (Å)		Pore volume (cm^3g^{-1})	
Wt% KCl	BET	BJH	DH	BJH	DH	BJH	DH
0.0	147.8	150.1	148.3	16.6	17.4	0.64	0.68
0.2	143.6	141.7	140.5	15.3	17.1	0.67	0.55
0.4	145.8	147.3	134.5	14.8	15.5	0.61	0.58
0.6	144.9	141.9	142.5	16.9	16.4	0.58	0.54
0.8	140.8	142.6	143.8	14.2	15.8	0.53	0.57
1.0	142.1	144.3	141.7	13.9	14.5	0.61	0.55
1.2	138.5	141.8	143.5	15.7	16.4	0.60	0.61

of the high CO conversion (70.9%), total selectivity to C_2-C_5 olefins (39.5%), low CO_2 (2.9%) and ∑Olefin/∑paraffin = 1.21.

CONCLUSIONS

Many variable factors are important such as Co/-Fe

Table 13. Effect of Different Total Pressures on Catalytic Performance of Optimal Nano Catalyst

	Pressure (bar)										
	1	3	5	7	9	11	13	15	17	20	25
CO conversion (%)	70.9	70.4	69.9	66.9	65.9	64.5	63.4	62.3	61.3	60.6	59.8
CH_4	13.3	13	12.6	12.0	11.8	11.5	11.1	10.6	10.4	10.6	10.2
C_2-C_3 paraffin	21.8	20.6	20.1	19.2	18.6	16.7	15.4	14.1	11.4	9.0	8.1
C_2-C_3 olefin	28.3	25.5	23.4	20.5	19.2	17.4	15.4	12.0	9.7	7.1	5.7
C_4-C_5 paraffin	10.8	11.9	12.6	13.4	14.1	14.6	15.3	16.1	16.4	16.6	17.2
C_4-C_5 olefin	11.2	13.0	12.8	13.8	14.4	15.1	15.7	17.5	16.8	17.6	17.5
C_6+	11.7	12.8	15	17.4	18.5	21.1	23.4	26.8	32.4	35.9	38
CO_2	2.9	3.2	3.5	3.7	3.4	3.6	3.7	2.9	2.9	3.2	3.3
∑Olefin/∑paraffin	1.21	1.18	1.11	1.06	1.03	1.04	1.01	0.98	0.95	0.97	0.92
Carbon balance (%)	97.6	97.1	96.8	97.5	96.1	96.3	95.1	96.6	94.9	96.4	97.1

Reaction conditions: $H_2/CO = 2/1$, GHSV = 1200 h^{-1} and 250 °C.

wt%, different Co/Fe ratios and KCl wt% in the preparation of the catalyst during catalyst preparation and FTS. The catalytic performances of optimal nano catalyst were investigated under different reaction conditions. The optimal reaction conditions for 50 wt% (Co/Fe)/SiO_2 (Co/Fe ratio is 70/30) nano catalyst promoted with 0.6 wt% KCl as optimal catalyst were: T = 250 ºC with molar feed ratio of H_2/CO = 2/1, GHSV = 1200 h^{-1} under 1 bar of total pressure. The optimal catalyst was found to be superior to the other catalysts in terms of catalytic activity (based on CO conversion) probably due to the facile formation of iron carbide during FTS reaction that is essential for light olefin production. In addition, methane production by using the 50 wt% (Co/Fe)/SiO_2 (Co/Fe ratio is 70/30) nano catalyst promoted with 0.6 wt% KCl was suppressed, which caused decreasing of methane selectivity from 25.6% for non promoted catalyst (50 wt% (Co/Fe)/SiO_2) to 13.3% for promoted catalyst.

ACKNOWLEDGMENTS

We thank the Razi University Research Council and Iran National Science Foundation (INSF) for support of this work.

REFERENCES

[1] Davis, B. H., Fischer-Tropsch synthesis: relationship between iron catalyst composition and process variables. *Catal. Today.* **2003**, *84*, 83-98, DOI: 10.1016/S0920-5861(03)00304-3.

[2] Feyzi, M.; Hassankhani, A., Synthesis, characterization and catalytic performance of nanosized iron-cobalt catalysts for light olefins production. *J. Nat. Gas. Chem.* **2011**, *20*, 677-686. DOI: 10.1016/S1003-9953(10)60241-1.

[3] Lari, T. T.; Mirzaei, A. A., Atashi, H. Fischer-

Tropsch Synthesis: Effects of aging time and operating temperatures on solvothermally prepared nanocatalyst for light olefin selectivity. *Catal. Lett.* **2017**, *14*, 71221-1234. DOI: 10.1007/s10562-017-2019-3.

[4] Dry, M. E., The Fischer-Tropsch process: 1950-2000, *Catal. Today*. **2002**, *71*, 227-241. DOI: 10.1016/S0920-5861(01)00453-9.

[5] Kwack, S. -H.; Bae, J. W.; Park, M. -J.; Kim, S. -M.; Ha, K. -S.; Jun, K. -W., Reaction modeling on the phosphorous-treated Ru/Co/Zr/SiO_2 Fischer-Tropsch catalyst with the estimation of kinetic parameters and hydrocarbon distribution. *Fuel.* **2011**, *90*, 1383-1394.

[6] Feyzi, M.; Norouzi, L.; Zamani, Y., Preparation and characterization of Fe-Co/SiO_2 nanocatalysts for gasoline range hydrocarbons production from syngas. *Catal. Lett.* **2016**, *146*, 1922-1933.DOI: 10.1007/s10562-016-1839-x.

[7] Pierre, A. C.; Pajonk, G. M., Chemistry of aerogels and their applications, *Chem. Rev.* **2002**, *102*, 4243-4266. DOI: 10.1021/cr0101306.

[8] Husing, N., Schubert, U. Aerogels-Airy materials: chemistry, structure and properties. *Angew. Chem. Int. Ed*. **1998**, *37*, 22-45. DOI: 10.1002/(SICI)1521-3773.

[9] Nurunnabi, M.; Murata, K.; Okabe, K.; Inaba, M.; Takahara, I., Performance and characterization of Ru/Al_2O_3 and Ru/SiO_2 catalysts modified with Mn for Fischer–Tropsch synthesis. *Appl. Catal. A: Gen.* **2008**, *340*, 203-211. DOI: 10.1016/ j.apcata.2008.02.013.

[10] He, M.; Xiao, B.; Hu, Z.; Liu, S.; Guo, X.; Luo, S., Syngas production from catalytic gasification of waste polyethylene: Influence of temperature on gas yield and composition. *Int. J. Hydrogen. Energy.* **2009**, *34*, 1342-1348. DOI: 10.1016/ j.ijhydene.2008.12.023.

[11] Feyzi, M.; Mirzaei, A. A., Performance and characterization of iron-nickel catalysts for light olefin production. *J. Natu. Gas. Chem.* **2010**, *19*, 422-430. DOI: 10.1016/S1003-9953(09)60092-X.

[12] Malek Abbaslou, R. M.; Tavassoli, A.; Soltan, J.; Dalai, A. K., Iron catalysts supported on carbon nanotubes for Fischer-Tropsch synthesis: Effect of catalytic site position. *Appl. Catal. A: Gen.* **2009**, *367*, 47-52. DOI: 10.1016/j.apcata.2009.07.025.

[13] Kim, D. J.; Dunn, B. C.; Huggins, F.; Huffman, G. P.; Kang, M. J.; Yie, E.; Eyring, E. M., SBA-15-supported iron catalysts for Fischer-Tropsch production of diesel fuel. *Ener. Fuels* **2006**, 202608-2611. DOI: 10.1021/ef060336f.

[14] Wu, B. S.; Bai, L.; Xiang, H. W.; Li, Y. W.; Zhang, Z. X.; Zhong, B., An active iron catalyst containing sulfur for Fischer-Tropsch synthesis. *Fuel.* **2004**, *83*, 205-212. DOI: 10.1016/S0016-2361(03)00253-9.

[15] Feyzi, M.; Khodaei, M. M.; Shahmoradi, J., Effect of preparation and operation conditions on the catalytic performance of cobalt-based catalysts for light olefins production. *Fuel. Proc. Tech.* **2012**, *93*, 90-98. DOI: 10.1016/j.fuproc.2011.09.021.

[16] Khodakov, A. Y.; Chu, W.; Fongarland, P., Advances in the development of novel cobalt Fischer-Tropsch catalysts for synthesis of long-chain hydrocarbons and clean fuels. *Chem. Rev,* **2007**, *107*, 1692-1744. DOI: 10.1021/cr050972v.

[17] Xiong, H.; Zhang, Y.; Liew, K.; Li, J., Fischer-Tropsch synthesis: The role of pore size for Co/SBA-15 catalysts. *J. Mol. Catal. A: Chem.* **2008**, *295*, 68-76. DOI: 10.1016/j.molcata.2008.08.017.

[18] Bae, J. W.; Kim, S. -M.; Kang, S. -H.; Chary, K. V. R.; Lee, Y. -J.; Kim, H. -J.; Jun, K. -W., Effect of support and cobalt precursors on the activity of Co/$AlPO_4$ catalysts in Fischer-Tropsch synthesis. *J. Mol. Catal. A: Chem.* **2009**, *311*, 7-16. DOI: 10.1016/j.molcata.2009.07.011.

[19] Iglesia, E., Design, synthesis, and use of cobalt-based Fischer-Tropsch synthesis catalysts. *Appl. Catal. A: Gen.* **1997**, *161*, 59-78. DOI: 10.1016/ S0926-860X(97)00186-5.

[20] Bian, G.; Mochizuki, T.; Fujishita, N.; Nomoto, H.; Yamada, M., Activation and catalytic behavior of several Co/SiO_2 catalysts for Fischer-Tropsch synthesis. *Ener. Fuels.* **2003**, *177*, 99-803. DOI: 10.1021/ef020236j

[21] Bianchi, C. L.; Martini, F.; Moggi, P., Co/SiO_2 sol-gel catalysts for Fischer-Tropsch synthesis. *Catal. Lett.* **2001**, *76*, 65-69. DOI: 10.1023/

A:1016712507527.

[22] Tristantini, D.; Lögdberg, S.; Gevert, B.; Borg, Ø.; Holmen, A., The effect of synthesis gas composition on the Fischer-Tropsch synthesis over Co/γ-Al_2O_3 and Co-Re/γ-Al_2O_3 catalysts. *Fuel. Proc. Tech.* **2007**, *88*, 643-649. DOI: 10.1016/j.fuproc.2007.01.012.

[23] Nurunnabi, M.; Murata, K.; Okabe, K.; Inaba, M.; Takahara, I., Effect of Mn addition on activity and resistance to catalyst deactivation for Fischer–Tropsch synthesis over Ru/Al_2O_3 and Ru/SiO_2 catalysts. *Catal. Commun.* **2007**, *8*, 1531-1537. DOI: 10.1016/j.catcom.2007.01.008.

[24] Fricke, J.; Tillotson, T., Aerogels: production, characterization, and applications, *Thin. Solid. Films.* **1997**, *297*, 212-223. DOI: 10.1016/S0040-6090(96)09441-2.

[25] Li, S.; Meitzner, G. D.; Iglesia, E., Structure and site evolution of iron oxide catalyst precursors during the Fischer-Tropsch synthesis. *J. Phys. Chem. B.* **2001**, *105*, 5743-5750. DOI: 10.1021/jp010288u.

[26] Riedel, T.; Schulz, H.; Schaub, G.; Jun, K. -W.; Hwang, J. -S.; Lee, K. -W., Fischer-Tropsch on iron with H_2/CO and H_2/CO_2 as synthesis gases: The episodes of formation of the Fischer-Tropsch regime and construction of the catalyst. *Top. Catal.* **2003**, *26*, 41-54. DOI: 1022-5528/03/1200-0041.

[27] Motjope, T. R.; Dlamini, H. T.; Hearne, G. R.; Coville, N. J., Application of in situ Mössbauer spectroscopy to investigate the effect of precipitating agents on precipitated iron Fischer-Tropsch catalysts. *Catal. Today.* **2002**, *71*, 335-341. DOI: 10.1016/S0920-5861(01)00460-6.

[28] Nakhaei Pour, A.; Kamali Shahri, S. M.; Bozorgzadeh, H. R.; Zamani, Y.; Tavasoli, A.; Marvast, M. A., Effect of Mg, La and Ca promoters on the structure and catalytic behavior of iron-based catalysts in Fischer–Tropsch synthesis. *Appl. Catal. A: Gen.* **2008**, *348*, 201-208. DOI: 10.1016/j.apcata.2008.06.045.

[29] Brady, R. C.; Pettit, R., Reactions of diazomethane on transition-metal surfaces and their relationship to the mechanism of the Fischer-Tropsch reaction. *J. Am. Chem. Soc.* **1980**, *102*, 6181-6182. DOI: 10.1021/ja00539a053.

[30] Ganesan, P.; Kuo, H. K.; Saaverda, A.; De Angelis, R. J., Particle size distribution function of supported metal catalysts by X-ray diffraction. *J. Catal.* **1978**, *52*, 310-320. DOI: 10.1016/0021-9517(78)90145-8.

[31] Uvarov, V.; Popov, I., Metrological characterization of X-ray diffraction methods for determination of crystallite size in nano-scale materials. *Mater. Charact.* **2007**, *58*, 883-891. DOI: 10.1016/j.matchar.2006.09.002.

[32] Bezemer, G. L.; Bitter, J. H.; Kuipers, H. P. C. E.; Oosterbeek, H.; Holewijn, J. E.; Xu, X.; Apteijn, F.; Van Dillen, A. J.; De Jong, K. P., Cobalt particle size effects in the Fischer-Tropsch reaction studied with carbon nanofiber supported catalysts. *J. Am. Chem. Soc.* **2006**, *128*, 3956-3964. DOI: 10.1021/ja058282w.

[33] Chernavskii, P. A.; Khodakov, A. Y.; Pankina, G. V.; Girardon, J. S.; Quinet, E., In situ characterization of the genesis of cobalt metal particles in silica-supported Fischer-Tropsch catalysts using Foner magnetic method. *Appl. Catal. A: Gen.* **2006**, *306*, 108-119. DOI: 10.1016/j.apcata.2006.03.033.

[34] Lermontov, A. S.; Girardon, J. -S.; Griboval-Constant, A.; Pietrzyk, S.; Khodakov, A. Y., Chemisorption of C_3 hydrocarbons on cobalt silica supported Fischer-Tropsch catalysts, *Catal. Lett.* **2005**, *101*, 117-126. DOI: 10.1007/s10562-005-3759-z.

[35] Bezemer, G. L.; Falke, U.; van Dillen, A. J.; De Jong, K. P., Cobalt on carbon nanofiber catalysts: auspicious system for study of manganese promotion in Fischer-Tropsch catalysis. *Chem. Commun.* **2005**, *6*, 731-733. DOI: 10.1039/B414788J.

[36] Iglesia, E.; Reyes, S. C.; Madon, R. J.; Soled, S. L., Selectivity control and catalyst design in the Fischer-Tropsch synthesis: Sites, Pellets, and Reactors. *Adv. Catal.* **1993**. *39*, 221-302. DOI: 10.1016/S0360-0564(08)60579-9.

[37] Schulz, H.; Vien Steen, E.; Claeys, M., Selectivity and mechanism of Fischer-Tropsch synthesis with iron and cobalt catalysts. *Stud. Surf. Sci. Catal.*

1994, *81*, 455-460. DOI: 10.1016/S0167-2991(08)63911-7.

[38] Schulz, H.; Claeys, M., Reactions of α-olefins of different chain length added during Fischer-Tropsch synthesis on a cobalt catalyst in a slurry reactor. *Appl. Catal. A: Gen.* **1999**, *186*, 71-90. DOI: 10.1016/S0926-860X(99)00165-9.

[39] Bukur, D. B.; Lang, X.; Akgerman, A.; Feng, Z., Effect of process conditions on olefin selectivity during conventional and supercritical Fischer-Tropsch synthesis. *Ind. Eng. Chem. Res.* **1997**, *36*, 2580-2587. DOI: 10.1021/ie960507b.

[40] Soled, S.; Iglesia, E.; Miseo, S.; DeRites, B. A.; Fiato, R. A., Selective synthesis of α-olefins on Fe-Zn Fischer-Tropsch catalysts. *Top. Catal.* **1995**, *2*, 193-205. DOI: 10.1007/BF01491967.

[41] Feyzi, M.; Babakhanian, A.; Gholivand, M. B., Catalytic performance and characterization of cobalt-nickel nano catalysts for CO hydrogenation. *Korean J. Chem. Eng.* **2014**, *31*, 37-44. DOI: 10.1007/s11814-013-0186-5.

[42] Jothimurugesan, K; Goodwin, Jr. J. G.; Gangwal, S. K.; Spivey, J. J., Development of Fe Fischer-Tropsch catalysts for slurry bubble column reactors. *Catal Today.* **2000**, *58*, 335-344. DOI: 10.1016/S0920-5861(00)00266-2.

[43] Nakhaei Pour, A.; Zamani, Y.; Tavasoli, A.; Kamali Shahri, S. M.; Taheri, S. A., Study on products distribution of iron and iron-zeolite catalysts in Fischer-Tropsch synthesis. *Fuel.* **2008**, *87*, 2004-2012. DOI: 10.1016/j.fuel.2007.10.014.

[44] Yang, Y.; Xiang, H. W.; Tian, L.; Wang, H.; Zhang, C. H.; Tao, Z. C.; Xu Y. Y.; Zhong, B.; Li, Y. W., Structure and Fischer-Tropsch performance of iron-manganese catalyst incorporated with SiO_2. *Appl. Catal. A: Gen.* **2005**, *284*, 105-122. DOI: 10.1016/j.apcata.2005.01.025.

[45] Bukur, D. B.; Mukesh, D.; Patel, S. A., Promoter effects on precipitated iron catalysts for Fischer-Tropsch synthesis. *Ind. Eng. Chem. Res.* **1990**, *29*, 194-204. DOI: 10.1021/ie00098a008.

[46] Shroff, M. D.; Kalakkad, D. S.; Coulter, K. E.; Kohler, S. D.; Harrington, M. S.; Jackson, N. B.; Sault, A. G.; Datye, A. K., Activation of precipitated iron Fischer-Tropsch synthesis catalysts. *J. Catal.* **1995**, *156*, 185-207. DOI: 10.1006/jcat.1995.1247.

[47] Borg, Ø.; Hammer, N.; Enger, B. C.; Myrstad, R.; Lindvag, O. A.; Eri, S.; Skagseth, T. H.; Rytter, E., Effect of biomass-derived synthesis gas impurity elements on cobalt Fischer-Tropsch catalyst performance including in situ sulphur and nitrogen addition. *J. Catal.* **2011**, *279*, 163-173. DOI: 10.1016/j.jcat.2011.01.015.

[48] Ragaini, V.; Carli, R.; Bianchi, C. L.; Lorenzetti, D.; Vergani, G., Fischer-Tropsch synthesis on alumina-supported ruthenium catalysts I. Influence of K and Cl modifiers. *Appl. Catal. A: Gen.* **1996**, *139*, 17-29. DOI: 10.1016/0926-860X(95)00331-2.

[49] Barrault, J. V., Forguyc. Effects of manganese oxide and sulphate on olefin selectivity of iron supported catalysts in the Fischer-Tropsch reaction. *Appl. Catal. A. Gen.* **1983**, *5*, 119-125. DOI: 10.1016/0166-9834(83)80300-5.

[50] Griboval-Constant, A.; Khodakov, A. Y.; Bechara, R.; Zholobenko, V. L., Support mesoporosity: a tool for better control of catalytic behavior of cobalt supported Fischer Tropsch catalysts. *Stud. Surf. Sci. Catal.* **2002**, *144*, 609-616. DOI: 10.1016/S0167-2991(02)80187-2.